Separation Science and Technology
Publication details, including instructions for authors and subscription information:
http://www.informaworld.com/smpp/title~content=t713708471

A Case Study of Realistic Two-Scale Modeling of Water Permeability in Fibrous Media

Sudhakar Jaganathan[a]; Hooman Vahedi Tafreshi[b]; Behnam Pourdeyhimi[a]
[a] Nonwovens Cooperative Research Center, NC State University, Raleigh, NC, USA [b] Mechanical Engineering Department, Virginia Commonwealth University, Richmond, Virginia, USA

To cite this Article Jaganathan, Sudhakar , Tafreshi, Hooman Vahedi and Pourdeyhimi, Behnam(2008) 'A Case Study of Realistic Two-Scale Modeling of Water Permeability in Fibrous Media', Separation Science and Technology, 43: 8, 1901 — 1916
To link to this Article: DOI: 10.1080/01496390802063960
URL: http://dx.doi.org/10.1080/01496390802063960

Separation Science and Technology, 43: 1901–1916, 2008

ISSN: 0149-6395 print/1520-5754 online
DOI: 10.1080/01496390802063960

Taylor & Francis
Taylor & Francis Group

A Case Study of Realistic Two-Scale Modeling of Water Permeability in Fibrous Media

Sudhakar Jaganathan,[1] Hooman Vahedi Tafreshi,[2] and Behnam Pourdeyhimi[1]

[1]Nonwovens Cooperative Research Center, NC State University, Raleigh, NC, USA
[2]Mechanical Engineering Department, Virginia Commonwealth University, Richmond, Virginia, USA

Abstract: There are several 3-D analytical models available for predicting the permeability of fibrous media. These models are developed based on the assumption that the medium is homogeneous with fibers oriented either in one specific direction, randomly oriented in the plane of the material, or isotropically oriented in a 3-D space. Unlike the homogeneous geometries normally considered for modeling, real media have a rather inhomogeneous Solid Volume Fraction (SVF), fiber orientations, and/or diameters. The presence of such non-uniformities in a real medium renders the models' predictions inaccurate. Sectioning-imaging, MRI imaging, or tomographic methods are often used to obtain a 3-D image of the real media for the purpose of calculating the permeability. These techniques, however, require extensive computational resources making the simulations limited to very small sub-domains. To circumvent this problem (required computational memory), a two-scale modeling approach is proposed that allowed modeling the entire thickness of a typical hydroentangled fabric on a personal computer. In particular, the micro-scale water permeability of a carded, hydroentangled nonwoven is computed via a finite difference CFD code, GeoDict, by using 3-D reconstructed microstructures obtained from Digital Volumetric Imaging (DVI). The resulting permeability tensors are then used in a lumped porous media model developed by Fluent Inc. for simulating water flow through the entire thickness of the material and the calculation of effective permeability. The modeling strategy presented in this study, is not limited to the case considered here and can be applied to different porous materials.

Keywords: CFD simulation, 3-D imaging, Permeability, Fibrous materials, Fiber, Nonwovens

Received 19 September 2007; accepted 11 February 2008.
Address correspondence to Hooman Vahedi Tafreshi, Mechanical Engineering Department, Virginia Commonwealth University, Richmond, VA 23284-3015, USA; Tel.: 804-828-9936; Fax: 804-827-7030; E-mail: htafreshi@vcu.edu

INTRODUCTION

Fibrous materials are widely used in industry as well as in our daily life for a very simple reason; they are flexible, relatively strong, and, most importantly, permeable. In almost all the applications where a fibrous material is deployed, its permeability is critically important. Viscous fluid flow through fibrous material has been often characterized using Darcy's law:

$$V = \mu^{-1} k \frac{\Delta p}{\Delta x} \tag{1}$$

where $V$is the superficial velocity, μ is the fluid viscosity, k is the permeability, and $\Delta p/\Delta x$ is the pressure drop per unit thickness. Using idealized modeled geometries many authors have proposed various expressions for predicting the permeability of fibrous materials (1–18). However, all these works are based on the assumption that the material is a homogeneous medium. On the contrary, real fibrous materials are rather inhomogeneous. The inhomogeneity can be in Solid Volume Fraction (SVF), in fiber orientations, and/or in fiber diameter distribution. These inhomogeneities can cause the permeability of a given specimen to be markedly different from what the models predict.

There are basically three different techniques for obtaining realistic information regarding the microstructure of a fibrous porous medium: serial sectioning-imaging of the material impregnated with a polymeric resin (19); Magnetic Resonance Imaging (MRI) (20), and X-Ray computed tomography (21–22). The 3-D geometries obtained via each of the above techniques can be used as a solution domain for solving fluid flow equations and calculating the materials' permeability. However, the resulting microstructures, especially when imaged at high resolutions, require enormous amount of computational memory which renders the above modeling strategy impractical. Our objective in this paper is to present a dual-scale modeling approach that allows utilizing real 3-D microstructures in calculating the permeability of a fibrous material without requiring significant computational resources. In this paper, we use an automated serial sectioning-imaging technique to obtain 3-D images of the microstructure of a hydroentangled fibrous media. Sub-domains of the large image are then used to derive the permeability of the material at micros-scales. The microstructural permeability constants are utilized in macro-scale model developed based on the lumped porous media model of the Fluent CFD code to obtain the effective permeability of the entire fabric using an ordinary personal computer.

Below, we provide a brief introduction to the automated sectioning-imaging technique considered in this paper. In section 3, we present the

micro-structural permeability modeling of a nonwoven fibrous material. In section 4, we compare micro-structural permeability with various permeability models presented in the literature. In section 5, we find the effective permeability of the entire hydroentangled fabric using a macro-scale model. This discussion is then followed by our conclusions in section 6.

DIGITAL VOLUMETRIC IMAGING TECHNIQUE

Digital Volumetric Imaging (DVI) [Micro-science Group Inc.], is a block-face fluorescence imaging technique (23). Here a fibrous material, embedded in a polymeric resin, is repeatedly sectioned and imaged automatically. These 2-D cross-sectional images are then combined to construct a 3-D image of the microstructure. Unlike the conventional serial sectioning methods which are laborious, serial sectioning in DVI is fully automated. The resolution of images obtained from DVI ranges from 0.48 to 4.48 μm/pixel, with a field of view ranging from 0.45 to 4.4 mm. The 3-D images can also be used for structural analysis (see Kerschmann (24) for more information).

For the current study, hydroentangled nonwoven fabrics made up of Nylon fibers with a fiber length of 3 cm and an average diameter of about 15 μm were produced in the pilot facilities of the Nonwovens Cooperative Research Center (NCRC) at NC State University. Hydroentangling is one of the most popular methods used for bonding loose fibers in a nonwoven fiber-web. The underlying mechanism in hydroentanglement is the exposure of the fibers to a non-uniform spatial pressure field created by successive banks of closely-packed high-speed waterjets. The impact of the waterjets with the fibers in a fiber-web displaces and rotates them with respect to their neighbors and result in fiber entanglement leading to a coherent and strong fabric (25–26). The fiber web used for the hydroentangling process here was prepared via a carding process.

Our hydroentangled fabric was stained using by Sulforhodamine 101 fluorescent dye and imaged using the DVI equipment. 600 cross-sectional images with a size of 800×800 pixels and a resolution of 1.77 μm/pixel were obtained. Figure 1 shows the reconstructed 3-D image considered for this study. Note that the resin used for impregnation has a low viscosity and we speculate that it did not cause significant change to microstructure, as it can be seen from Fig. 1. We measured the thickness of the sample by using the 3-D image obtained from DVI and the original fabric according to the ASTM D5729 test procedure. These two measurements showed a relatively good agreement.

Figure 1. 3-D reconstructed DVI image of a typical carded hydroentangled nonwovens ($800 \times 800 \times 600$ voxels, with a resolution of 1.77 μm/pixel and an average fiber diameter of about 15 μm).

MICROSCALE PERMEABILITY MODELING

The problem in using real microstructures in fluid mechanics computation is the complexity of the solution domain. In this paper, we used the grid-aligned version of the Peskin's Immersed Boundary Method (IBM) implemented in the GeoDict CFD code from ITWM, Germany (27–28). By binirizing the 3-D images and converting the pore space into empty cells and the fibers into solid obstacles, one can use the image voxels as the computational cells. This greatly reduces the difficulties involved in mesh generation of complex geometries.

A finite difference scheme was used to solve steady state Stokes equation with periodic boundary condition. In this scheme velocity variables are assigned to the voxel faces and the pressure variables are defined at the center of each voxel. The governing equations for conservation of mass and momentum are given below respectively:

$$\frac{\partial v_x}{\partial x} + \frac{\partial v_y}{\partial y} + \frac{\partial v_z}{\partial z} = 0 \tag{2}$$

$$\frac{\partial p}{\partial x} = \mu\left(\frac{\partial^2 v_x}{\partial x^2} + \frac{\partial^2 v_x}{\partial y^2} + \frac{\partial^2 v_x}{\partial z^2}\right) \tag{3.1}$$

$$\frac{\partial p}{\partial y} = \mu\left(\frac{\partial^2 v_y}{\partial x^2} + \frac{\partial^2 v_y}{\partial y^2} + \frac{\partial^2 v_y}{\partial z^2}\right) \tag{3.2}$$

$$\frac{\partial p}{\partial z} = \mu\left(\frac{\partial^2 v_z}{\partial x^2} + \frac{\partial^2 v_z}{\partial y^2} + \frac{\partial^2 v_z}{\partial z^2}\right) \tag{3.3}$$

where v_x,v_y, and v_z are velocity in the x, y, and z directions, respectively, and p and μ are pressure and viscosity respectively. Our simulation strategy here is to specify a pressure drop in a given direction and then obtain the averaged flow velocity through the fibrous medium. Pressure drops were chosen such that velocity is always below 0.01 m/s resulting in Reynolds numbers smaller than unity (Stokes flow). Note that the periodic boundary conditions considered in our simulations results in non-zero velocity components in the lateral directions (perpendicular to the applied pressure gradient).

According to the Darcy's law we have:

$$v_x = \frac{1}{\mu}\left(k_{xx}\frac{\partial p}{\partial x} + k_{xy}\frac{\partial p}{\partial y} + k_{xz}\frac{\partial p}{\partial z}\right) \tag{4.1}$$

$$v_y = \frac{1}{\mu}\left(k_{yx}\frac{\partial p}{\partial x} + k_{yy}\frac{\partial p}{\partial y} + k_{yz}\frac{\partial p}{\partial z}\right) \tag{4.2}$$

$$v_z = \frac{1}{\mu}\left(k_{zx}\frac{\partial p}{\partial x} + k_{zy}\frac{\partial p}{\partial y} + k_{zz}\frac{\partial p}{\partial z}\right) \tag{4.3}$$

where here $k_{ij}(i,j = x,y,z)$ is the full permeability tensor of the subdomain. Note that by specifying a value to the pressure gradient along one of the Cartesian coordinates, while others are set to zero, one can obtain three elements of the permeability tensor. Repeating this procedure for the other two coordinate directions, all the 9 elements of the k_{ij} tensor will be obtained.

MICROSCALE PERMEABILITY CONSTANTS

Analytical Models to Predict Microscale Permeability

Existing analytical or numerical models consider the microstructure of a fibrous medium to be either of "unidirectional", "layered" or "isotropic random" as shown in Fig. 2. Here, for simplicity, we assume the so-called machine direction (MD) to be in the y-direction. The x- and z-directions, therefore, will be the cross-machine and through-plane (or thickness) directions, respectively, and shown by CD and TD. "Unidirectional" is

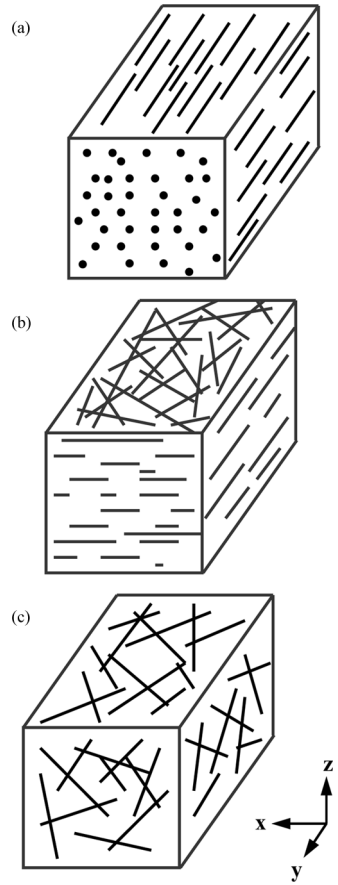

Figure 2. A schematic representation of various permeability models a) Unidirectional random fiber arrangement, b) Layered fiber arrangement, c) Random fiber arrangement.

the case where fiber axes lie parallel or perpendicular to flow direction. The medium's microstructural permeability constants in the y, x, and z directions are therefore, shown by k_{MD}^{und}, k_{CD}^{und}, and k_{TD}^{und}, respectively. Note that $k_{CD}^{und} = k_{TD}^{und}$. Fibrous structure can be classified as "layered" if fiber axes lie randomly in planes perpendicular to the flow direction. In this type of structure, permeability constants are k_{MD}^{lay}, k_{CD}^{lay}, and k_{TD}^{lay} where $k_{MD}^{lay} = k_{CD}^{lay}$ and are normally greater than k_{TD}^{lay}. "Isotropic random" is the case where fiber axes is randomly orientated in all the three coordinate directions. In this case, there exist only one permeability constant of $k_{MD}^{ran} = k_{CD}^{ran} = k_{TD}^{ran}$.

Using Brinkman's equation, Speilman and Goren (3) proposed different expressions for the permeability of modeled fibrous media. Their expressions for flow perpendicular, k_{TD}^{lay} and parallel, $k_{MD}^{lay} = k_{CD}^{lay}$, to a layered microstructure, are:

$$\frac{1}{4\phi} = \frac{1}{2} + \frac{\sqrt{k_{TD}^{lay}}}{r} \frac{K_1\left(\frac{r}{\sqrt{k_{TD}^{lay}}}\right)}{K_2\left(\frac{r}{\sqrt{k_{TD}^{lay}}}\right)} \tag{5}$$

$$\frac{1}{4\phi} = \frac{1}{4} + \frac{3}{4}\frac{\sqrt{k_{CD}^{lay}}}{r} \frac{K_1\left(\frac{r}{\sqrt{k_{CD}^{lay}}}\right)}{K_2\left(\frac{r}{\sqrt{k_{CD}^{lay}}}\right)} \tag{6}$$

where K_1 and K_2 are Bessel functions of second kind, r is the fiber radius and ϕ is the solid volume fraction. It is worth mentioning that in 1952 Davies (29) developed an empirical correlation which has been widely used since for filter media. The Davies's correlation is in good agreement with the above expression of Speilman and Goren (Eq. (5)) for the range of SVFs considered in this paper and so is not shown here for the sake of brevity.

Speilman and Goren (3) also derived the following expression for flow through isotropic random microstructures, $k_{MD}^{ran} = k_{CD}^{ran} = k_{TD}^{ran}$.

$$\frac{1}{4\phi} = \frac{1}{3} + \frac{5}{6}\frac{\sqrt{k_{TD}^{ran}}}{r} \frac{K_1\left(\frac{r}{\sqrt{k}}\right)}{K_2\left(\frac{r}{\sqrt{k}}\right)} \tag{7}$$

For the case of flow parallel to fibers in unidirectional microstructures, Speilman and Goren (3) proposed the following expression.

$$\frac{1}{4\phi} = \frac{1}{2}\frac{\sqrt{k_{MD}^{und}}}{r} \frac{K_1\left(\frac{r}{\sqrt{k_{MD}^{und}}}\right)}{K_2\left(\frac{r}{\sqrt{k_{MD}^{und}}}\right)} \tag{8}$$

Speilman and Goren (3) did not make a distinction between the case of flow perpendicular to the fibers in unidirectional fiber bundles, $k_{CD}^{und} = k_{TD}^{und}$, and that perpendicular to a layered microstructure, k_{TD}^{lay}.

Note that many authors have proposed analytical or numerical expressions to predict the permeability of unidirectional microstructures in CD or TD directions. Kuwabara (2) and Sangani and Acrivos (3), Drummond and Tahir (5), studied the case of cross flow in fiber bundles with a regular fiber arrangement, and are known for under-predicting the permeability of 3-D fibrous structure (11,30). In a recent study, Chen and Papathanasiou (31) studied the case of flow parallel and perpendicular to fiber bundles in 2-D and have reported on their permeability calculations at high SVFs. Previously, we have shown that 2-D modeling of Papathanasiou and his co-workers (9), same as other 2-D models, underpredict the medium's permeability at low SVFs (32). Tomadakis and Robertson (15) have also reported on a comprehensive 3-D permeability modeling accounting various fiber orientations. Comparing the results of Tomadakis and Robertson (15) with the well known empirical correlation of Davies (29) (the most reliable experimental permeability correction available) revealed that their expressions over-predict the permeability of real fibrous media for the range of SVFs considered in this paper. We, therefore, used the expressions of Spielman and Goren (3) which is probably the most accurate analytical predictive model available for the range of SVFs considered here.

Microscale Permeability of A Typical Carded Hydroentangled Nonwoven

As mentioned in section 2, in the current study, we considered a nonwoven fabric obtained by hydroentangling a carded fiberweb of Nylon fibers with a length of 3 cm and an average diameter of about 15 μm. Local (microscale) permeability constants of the specimen shown in Fig. 1 (with a size of $800 \times 800 \times 600$) can be found by taking a series of sub-domains from the original 3-D image and solving Eqs. (2) and (3) using the GeoDict code. In order to find an appropriate size for the simulation domain we used the Brinkman screening length. According to Clague and Philip (8) and Clague et al. (13), a simulation domain greater than the Brinkman length, $\sqrt{k}$ (where k is permeability of the medium), by a factor of 14 is sufficiently large to smooth out the effect of local inhomogeneities. Since no prior knowledge of the medium's permeability was available, we used the Spielman and Goren (Eq. (7)) to approximate the size of the simulation domain. In this paper, we considered a series of sub-domains with a size of $200 \times 200 \times 200$ voxels. This is large enough to represent the microscale properties of our fibrous media and, at the same time, small enough to allow the computations to be carried out on a personal computer. Figure 3 shows a typical sub-domain used in this study.

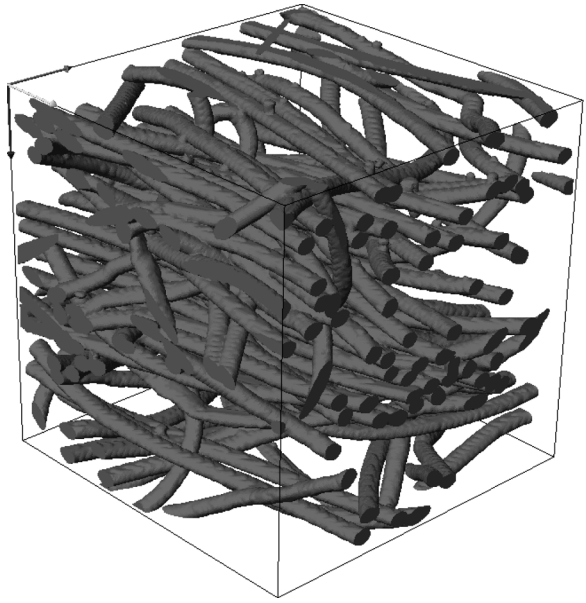

Figure 3. A sub-domain of DVI image used in finite difference calculations.

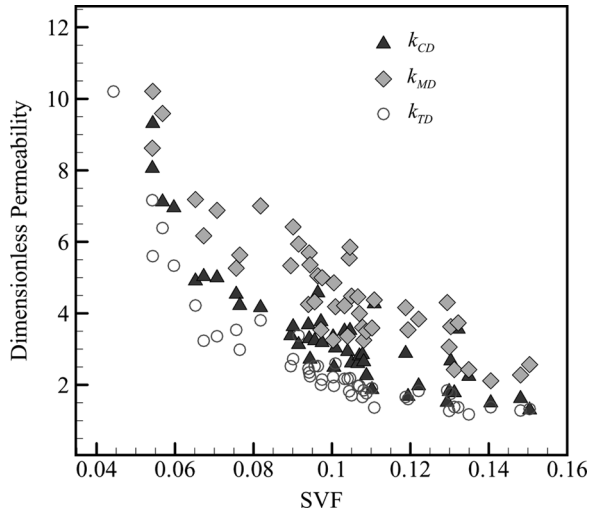

Figure 4. Permeability of microstructure as a $f(\phi)$ in main flow direction (k_{TD}, k_{MD}, k_{CD}).

In Fig. 4, the local permeability constants obtained form simulating a series of sub-domains in the machine (k_{MD}), cross-machine (k_{CD}), and thickness (k_{TD}) directions are shown versus the SVF. Note that the resulting local permeability tensors are found to be almost symmetric with negligible off-diagonal elements when compared with the diagonal elements.

From Fig. 4, it may be observed that the local SVF considerably changes from one region to another within $800 \times 800 \times 600$ specimen resulting in different local permeability values. In this figure, note that k_{TD} is smaller than k_{CD} and k_{MD}. Interestingly, it can also be seen that k_{MD} is smaller than k_{CD} indicating that there is some degree of in-plane directionality in the material.

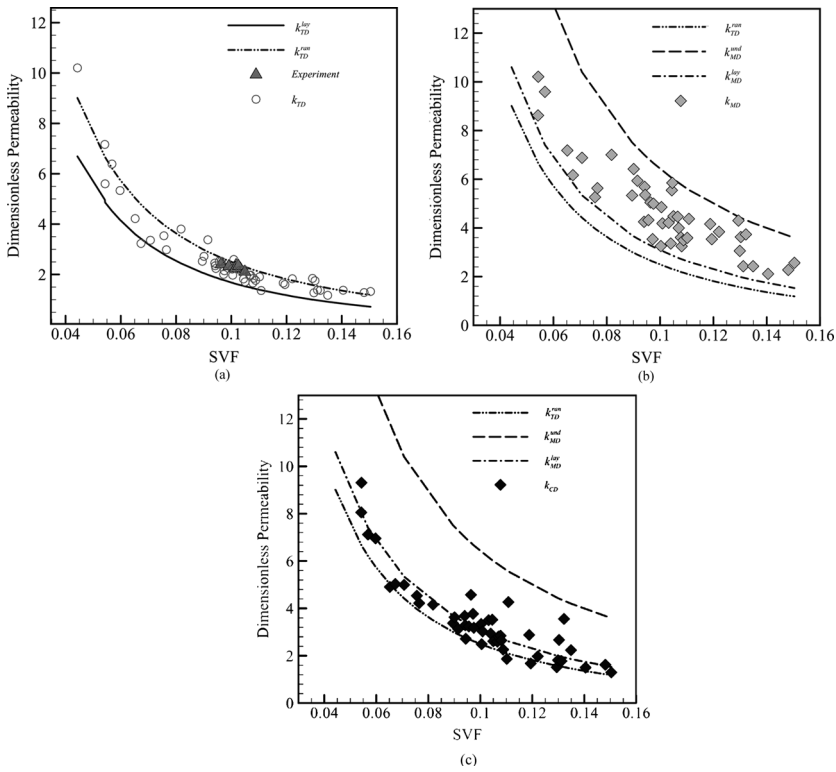

Figure 5. Comparison of micro-structural permeability with analytical expressions of Spielman and Goren (3), a) z-direction (TD) b) x-direction (CD) c) y-direction (MD).

The permeability in the TD direction tends to lie between k_{TD}^{lay} and k_{TD}^{ran} of Spielman and Goren (Eqs. (5) and (7), respectively), i.e., $k_{TD}^{und} < k_{TD}^{lay} < k_{TD} < k_{TD}^{ran}$, as it can be seen in Fig. 5a. In the MD direction, our permeability constants lie between k_{MD}^{lay} and k_{MD}^{und} (Eqs. (6) and (8), respectively), i.e., $k_{MD}^{ran} < k_{MD}^{lay} < k_{MD} < k_{MD}^{und}$, as it can be seen in Fig. 5b. Note that k_{MD} is closer to k_{MD}^{lay}, at low SVFs, indicating that the microstructure of our medium is less likely to be unidirectional at low SVFs.

In the CD direction, our permeability constants are somewhat scattered between all the three models making it difficult to distinguish clear upper and lower boundaries (see Fig. 5c). It, however, seems that our results are mostly close to k_{CD}^{lay} indicating a somewhat layered microstructure for the material used in this work.

It is worth mentioning that if the fibers were perfectly oriented in the MD direction, then one would expect to see $k_{TD}^{und} = k_{CD}^{und}$ which is not exactly the case here but, as shown in Fig. 4, there are some indications suggesting some degrees of unidirectionality in the fiber arrangement. This can probably be caused by the hydroentangling jet-streaks which form ridges and valleys on the surface of the fabric as discussed in our previous work (26).

The above analysis shows that existing idealized models may not always be sufficient for predicting the permeability of a fibrous material. Small deviations from an ideal fiber arrangement considered by the above models can bring about considerable error in the prediction. This requires developing future models that allow for the imperfection of the fiber arrangements (e.g., the 2-D work of Chen and Papathanasiou (31)).

MACROSCALE PERMEABILITY CONSTANTS

From a practical point of view the local permeability constants need to be converted to a single representative value – effective permeability. Obviously, the effective permeability would be found if one could simulate the entire thickness of the material (see Fig. 1). However, as mentioned earlier, such a simulation is computationally expensive. We, therefore, used the local permeability tensors obtained from Eq. (4) in a macroscale porous media model implemented in the Fluent CFD code to find the effective permeability of the material. A porous medium in Fluent is modeled by the addition of a momentum sink term to the fluid flow equation in a specified region of the solution domain. This momentum sink term is a viscous resistance ($W_{ij} = k_{ij}^{-1}$) which we found from our sub-domain modeling. These local permeability constants contribute

to a pressure gradient in each porous region creating an overall pressure drop for the whole domain. In our macroscale modeling, the finite volume method of Patankar (33) is exploited to solve the continuity and the Darcy's equation:

$$\frac{\partial v_x}{\partial x} + \frac{\partial v_y}{\partial y} + \frac{\partial v_z}{\partial z} = 0 \tag{12}$$

$$\nabla p_x = \mu W_{xx} v_x + \mu W_{xy} v_y + \mu W_{xz} v_z \tag{13.1}$$

$$\nabla p_y = \mu W_{yx} v_x + \mu W_{yy} v_y + \mu W_{yz} v_z \tag{13.2}$$

$$\nabla p_z = \mu W_{zx} v_x + \mu W_{zy} v_y + \mu W_{zz} v_z \tag{13.3}$$

where $W_{ij} = \frac{Co\text{–}factor\ k_{ij}}{\det k_{ij}} (i,j = x,y,z)$. The above equations are solved in each porous zone (lumped sub-domain) and so the permeability tensor

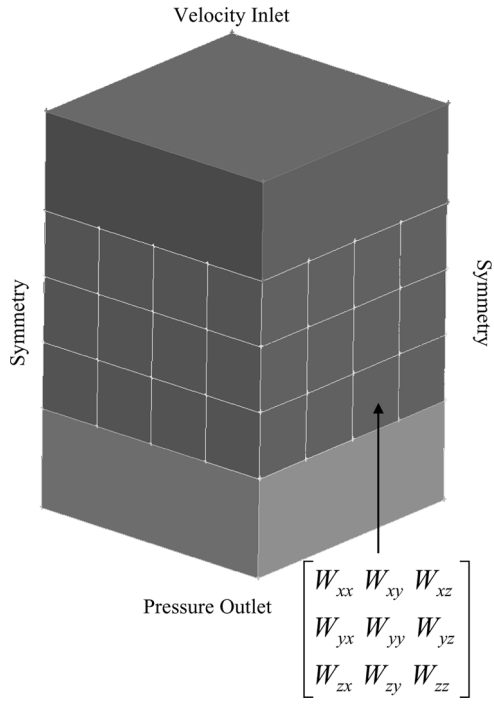

Figure 6. Simulation domain together with boundary conditions used to calculate effective permeability.

in each zone here is an input which was obtained from our sub-domain simulations (see section 3). Boundary conditions considered for the simulations are shown in Fig. 6. Symmetry boundary condition is considered for all the sides of the computational box. A fluid entry and exit zone was placed over the nonwoven material in a distance $L = 0.5\,t$ where t here is the thickness of the fibrous medium in the simulation box. This is to ensure that the pressure drop calculation is carried out in the regions far from any flow gradients. Water was used as fluid with superficial velocity of 0.01 m/s. Note that if the sample size is large enough, the choice of symmetry boundary conditions will not affect the simulation results. This is because flow is mainly in the through-plane direction and lateral flows are negligible.

A similar type of two-scale modeling has been carried out by Schweers and Löffler (19), and Lehmann et al. (34). However, these authors have used the over-simplified unidirectional fiber bundle model of Kuwabara in their calculation of effective permeability. As shown in this article, unidirectional models under-predict the permeability of a real fibrous microstructure and can render the effective permeability calculations inaccurate.

Macroscale Permeability of A Typical Carded Hydroentangled Nonwoven

Our aim here is to simulate the permeability of the entire thickness of our hydroentangled fabric. As mentioned earlier, we divided our $800 \times 800 \times 600$ image into 48 sub-domains of $200 \times 200 \times 200$ voxel and simulated their microscale permeabilities (see Fig. 5). The CPU time needed for running each of our 48 sub-domain simulations was around 90 minutes with a memory requirement of about 1 GB. These microscale permeability constants are now used in a lumped porous model to simulate the permeability of the whole medium. Our lumped model simulation required less than 2 GB of RAM and took about 30 minutes to converge. The dimensionless effective permeability obtained from this simulation was found to be 2.12.

In order to further validate our simulations, we measured the through-plane permeability of our fabric using a Frazier air permeability tester. A constant pressure drop of 0.5 inches of water was used in the experiment. The Reynolds number measured from the test ($\sim$0.7) was higher than the one used in the simulations ($\sim$0.16), but the inertial effects can still be ignored. A total of 30 tests were conducted which resulted in an average dimensionless permeability of about 2.19 with a Standard Deviation of 0.07. The individual data points are shown in

Fig. 5a. It can be seen that simulations are in good agreement with our experimental measurement. This hybrid technique of finding effective permeability based on realistic data obtained from the high resolution microstructure of fibrous structure together with porous media lumped models seems promising regarding efficiency and time consumption.

CONCLUSIONS

In this article, a two-scale approach for calculating the permeability of a porous medium was presented. By calculating the permeability of a series of microstructures obtained via 3-D DVI imaging, we simulated the macroscale permeability of a carded hydroentangled fabric by using a regular personal computer. Comparing our permeability simulations with experimental data indicate that our two-scale modeling is reasonably accurate and can be used in cases where a one-step simulation is not possible due to the extensive computational requirements.

As a case study, we considered a carded hydroentangled fabric and calculated its microscale and macroscale permeability constants. The microscale permeability calculations were compared with the most reliable analytical permeability models and were discussed in details.

ACKNOWLEDGEMENT

The current work is supported by the Nonwovens Cooperative Research Center. Their support is gratefully acknowledged.

REFERENCES

1. Happel, J. (1959) Viscous flow relative to arrays of cylinders. *A.I.Ch.E. Journal*, *15* (2): 174–177.
2. Kuwabara, S. (1959) The forces experienced by randomly distributed parallel circular cylinders of spheres in a viscous flow at small Reynolds number. *Journal of the Physical Society of Japan*, *14* (4): 527–532.
3. Spielman, L., Goren, S.L. (1968) Model for predicting pressure drop and filtration efficiency in fibrous media. *Environmental Science and Technology*, *2*: 279–287.
4. Sangani, A.S., Acrivos, A. (1982) Slow flow past periodic arrays of cylinders with application of heat transfer. *International Journal of Multiphase Flow*, *8*: 193–206.
5. Drummond, J.E., Tahir, M.I. (1984) Laminar viscous flow through regular arrays of parallel solid cylinders. *International Journal of Multiphase Flow*, *10* (3): 515–540.

6. Jackson, G.W., James, D.F. (1986) The permeability of fibrous porous media. *Canadian Journal of Chemical Engineering*, *64* (3): 364–374.
7. Higdon J.J.L., Ford, G.D. (1996) Permeability of three-dimensional models of fibrous porous media. *Journal of Fluid Mechanics*, *308*: 341–361.
8. Clague, S. D., Phillips, J.R. (1997) A numerical calculation of the hydraulic permeability of three dimensional disordered fibrous media. *Physics of Fluids*, *9* (6): 1562–1572.
9. Papathanasiou, T.D., Lee, P.D. (1997) Morphological effects on the transverse permeability of arrays of aligned fibers. *Polymer Composite*, *18* (2): 242–253.
10. Koponen, A., Kandhai, D., Hellén, E., Alava, M., Hoekstra, A., Kataja, M., Niskanen, K., Sloot, P., Timonen, J. (1998) Permeability of three dimensional random fiber webs. *Physical Review Letters*, *80* (4): 716–719.
11. Dhaniyala, S., Liu, B.Y.H. (1999) An asymmetrical, three-dimensional model for fibrous filters. *Aerosol Science and Technology*, *30*: 333–348.
12. Chase, G.G., Beniwal, V., Venkataraman, C. (2000) Measurement of uniaxial fiber angle in nonwoven fibrous media. *Chemical Engineering Science*, *55*: 2151–2160.
13. Clague, D.S., Kandhai, B.D., Zhang, R., Sloot, P.M.A. (2000) Hydraulic permeability of (un) bounded fibrous media using the lattice Boltzmann method. *Physical Review E*, *61* (1): 6616–6625.
14. Mao, N., Russell, S.J. (2003) Anisotropic liquid absorption in homogeneous two dimensional nonwoven structures. *Journal of Applied Physics*, *94* (6): 4135–4138.
15. Tomadakis, M. M., Robertson, J. T. (2005) Viscous permeability of random fiber structures: Comparison of electrical and diffusional estimates with experimental and analytical results. *Journal of Composite Materials*, *39* (2): 163–188.
16. Wang, Q., Maze, B., Vahedi Tafreshi, H., Pourdeyhimi, B. (2006) A Note on Permeability Simulation of Multifilament Woven Fabrics. *Chemical Engineering Science*, *61*: 8085.
17. Wang, Q., Vahedi Tafreshi, H., Maze, B., Pourdeyhimi, B. (2006) A case study of simulating submicron aerosol filtration via lightweight spun-bonded filter media. *Chemical Engineering Science*, *61*: 4871–4883.
18. Zobel, S., Maze, B., Vahedi Tafreshi, H., Wang, Q., Pourdeyhimi, B. (2007) Simulating Permeability of 3-D Calendered Fibrous Structures. *Chemical Engineering Science*, *62*: 6285–6296.
19. Schweers, E., Löffler, F. (1994) Realistic modeling of the behavior of fibrous filters through consideration of filter structure. *Powder Technology*, *80*: 191–206.
20. Hoferer, J., Hardy, E.H., Meyer, J., Kasper, G. (2007) Measuring particle deposition within fibrous filter media by magnetic resonance imaging. *Filtration*, *7* (2): 154–158.
21. Faessel, M., Delisée, C., Bos, F., Castéra, P. (2005) 3D modelling of random cellulosic fibrous network X-ray tomography and image analysis. *Composite Science and Technology*, *65*: 1931–1940.

22. Lux, J., Ahmadi, A., Gobbé, C., Delisée, C. (2006) Macroscopic thermal properties of real fibrous material: Volume averaging method and 3D image analysis. *International Journal of Heat and Mass Transfer*, *49*: 1958–1973.
23. Chinn, D., Ostendorp, P., Haugh, M., Kershmann, R., Kurfess, T., Claudet, A., Tucker, T. (2004) Three dimensional imaging of LIGA- made microcomponents. *Journal of Manufacturing Science and Engineering*, *126*: 813–821.
24. Kerschmann, R. (2001) Filter media structure in virtual reality. *Filtration & Separation*, *38* (7): 26–29.
25. Vahedi Tafreshi, H., Pourdeyhimi, B. (2003) Effects of nozzle geometry on waterjet breakup at high Reynolds numbers. *Experiments in Fluids*, *35* (4): 364.
26. Anantharamaiah, N., Vahedi Tafreshi, H., Pourdeyhimi, B. (2006) A study on hydroentangling waterjets and their impact forces. *Experiments in Fluids*, *41* (1): 103.
27. Jung, Y., Torquato, S. (2005). Fluid permeability of triply periodic minimal surfaces. *Physical Review E*, *72*: 056319.
28. Kim, J., Kim, D., Choi, H. (2001) An immersed-boundary finite volume method for simulation of flow in complex geometries. *Journal of Computational Physics*, *171*: 132–150.
29. Davies, C.N. (1952) The separation of airborne dust and particles. *Proceedings of Institute of Mechanical Engineers B1*; London, 185–213.
30. Rodman, C.A., Lessmann, R.C. (1988) Automotive nonwoven filter media: Their constructions and filter mechanism. *Tappi Journal*, *71*: 161–168.
31. Chen, X.M., Papathanasiou, T.D. (2007) Micro-scale modeling of axial flow through disordered fiber array. *Composite Science and Technology*, *67* (7–8): 1286–1293.
32. Jaganathan, S., Vahedi Tafreshi, H., Pourdeyhimi, B. (2008) A realistic approach for modeling permeability of fibrous media: 3-D imaging coupled with CFD. *Chemical Engineering Science*, *63*: 244–252.
33. Patankar, S.V. (1980) *Numerical Heat Transfer and Fluid Flow*; Hemisphere Pub.: Washington.
34. Lehmann, M.J., Hardy, E.H., Meyer, J., Kasper, G. (2005). Fibrous filters: Non-invasive determination of local 3D fiber structure by MRI. *Filtration*, *5* (2): 62–67.